Analysis of Embedded Shock Waves Calculated by Relaxation Methods

EARLL M. MURMAN*
NASA Ames Research Center, Moffett Field, Calif.

The requirements for uniqueness of the calculated jump conditions across embedded shock waves are investigated for type-dependent difference systems used in transonic flow studies. A mathematical analysis shows that sufficient conditions are: a) the equations should be differenced in conservative form; and b) a special difference operator should be used when switching from a hyperbolic to an elliptic operator. The latter results in a consistency condition on the integral equations, rather than the differential, at these points. Calculated jump conditions for several embedded and detached shock waves are analyzed in the physical and hodograph planes. Comparisons are made with previous results, a time-dependent calculation, and data.

I. Introduction

DURING the past several years, type dependent relaxation methods have been used to calculate steady inviscid transonic flows about a variety of aerodynamic shapes. Procedures have been developed for solving the transonic small-disturbance equations and full potential equations for two-dimensional and axisymmetric bodies and for the transonic small-disturbance equations for three-dimensional wings (see Ref. 1 for a survey). The results converge to accepted exact solutions for subcritical and shock-free supercritical flows. Results with embedded shocks agree well with experimental data, although the shock pressure rise on the surface is consistently less than the theoretical value for the normal shock. This fact had been attributed[2] to a smoothing out of the re-expansion singularity[3] by numerical truncation errors.

A discussion of the numerical shock structure in Ref. 4 explains the mechanism by which the finite-difference methods can approximate a discontinuous solution. No analysis has been given, however, to show that the resulting calculated jump uniquely satisfies the theoretical jump appropriate for the system of governing equations. A critical review of this deficiency has recently been presented by Yoshihara.[1] During the past year, the author and R. Magnus performed a detached bow-wave calculation using relaxation and time-dependent methods, respectively. The results show that the relaxation calculations give incorrect shock jumps for strong oblique shock waves.

The work presented here was undertaken to resolve this problem. An analysis has been completed which gives the correct finite-difference procedures to use to guarantee that the calculated shock jump uniquely satisfies the theoretical jump conditions.

II. Analysis

Governing Equations

The model equations to be used for analyzing the numerical techniques are based on transonic small-disturbance theory.[2] The simplest governing partial differential equation for two-dimensional flow which displays the basic mathematical features is

$$-(\tfrac{1}{2}\phi_x{}^2)_x+\phi_{yy}=0 \tag{1a}$$

or, equivalently

$$-\phi_x\phi_{xx}+\phi_{yy}=0 \tag{1b}$$

This nonlinear equation changes type from elliptic to hyperbolic as the local velocity perturbation ϕ_x passes through zero (sonic velocity). The divergence theorem may be used to obtain an integral relation that is equivalent to Eq. (1)

$$\int\int \nabla\cdot\mathbf{\Phi}\,dA=\int \mathbf{\Phi}\cdot\mathbf{n}\,ds=0 \tag{2}$$

where

$$\mathbf{\Phi}=(-\tfrac{1}{2}\phi_x{}^2)\hat{k}+\phi_y\hat{l}$$

Equation (1) is valid throughout the flowfield domain except on surfaces of discontinuity such as shock waves and vortex sheets. Shock-jump relations (weak solution) can be obtained from the integral relation (2) in the standard way. With $u\equiv\phi_x$ and $v\equiv\phi_y$, and 1 and 2 denoting the upstream and downstream states respectively, the jump relations are[2]

$$\tfrac{1}{2}(u_2+u_1)(u_2-u_1)^2-(v_2-v_1)^2=0 \tag{3}$$

or, equivalently

$$\tfrac{1}{2}(u_2{}^2-u_1{}^2)+\tan\theta_s(v_2-v_1)=0 \tag{4a}$$

$$\tan\theta_s=(dx/dy)_s=-[(v_2-v_1)/(u_2-u_1)] \tag{4b}$$

The potential function ϕ is continuous across a shock wave. Equation (3) is the transonic small-disturbance approximation to the Rankine-Hugoniot polar.

To solve a problem, suitable boundary conditions must be added to the previous equations to complete the formulation. These boundary conditions for specific problems are derived and discussed in the cited references. There are no general proofs for uniqueness or existence of the solutions of these equations.

Difference Equations

A computational procedure to solve Eq. (1) was introduced in Ref. 2 and developed further in Refs. 4 and 5. The procedure uses relaxation methods to solve finite-difference equations constructed from difference operators that are chosen at each mesh point based on the local type of Eq. (1). The method as developed to date is reviewed, followed by a new analysis of the calculated shock jumps.

With the standard difference notation, a centered difference operator at point ij may be written for Eq. (1a) (divergence form) as

$$-\tfrac{1}{2}\frac{(\phi_x{}^2)_{i+1/2,j}-(\phi_x{}^2)_{i-1/2,j}}{\Delta x}+\frac{(\phi_y)_{i,j+1/2}-(\phi_y)_{i,j-1/2}}{\Delta y}=0 \tag{5a}$$

Presented at the AIAA Computational Fluid Dynamics Conference, Palm Springs, Calif., July 19–20, 1973; submitted September 6, 1973; revision received November 19, 1973. The author wishes to acknowledge discussions with Y. Yoshihara and R. Magnus and the detached bow wave computation furnished by them. Several calculations in the paper were performed by M. Johnson of the Computer Sciences Corp.

Index categories: Subsonic and Transonic Flow; Aircraft Aerodynamics (Including Component Aerodynamics).

* Research Scientist. Member AIAA.

Upon substituting the relations

$$\phi_{x_{i+1/2,j}} \equiv \frac{\phi_{i+1,j}-\phi_{i,j}}{\Delta x} \equiv u_{i+1/2,j}$$
$$\phi_{y_{i,j+1/2}} \equiv \frac{\phi_{i,j+1}-\phi_{i,j}}{\Delta y} \equiv v_{i,j+1/2} \text{ etc.} \quad (6)$$

and factoring, we get

$$-\left(\frac{\phi_{i+1,j}-\phi_{i-1,j}}{2\Delta x}\right)\left[\frac{\phi_{i+1,j}-2\phi_{ij}+\phi_{i-1,j}}{(\Delta x)^2}\right]+$$
$$\left[\frac{\phi_{i,j+1}-2\phi_{ij}+\phi_{i,j-1}}{(\Delta y)^2}\right]=0 \quad (5b)$$

This equation is a suitable second-order accurate difference operator for an elliptic equation of the Laplace type. Hence, if the term in the first bracket (centered velocity formula)

$$\phi_{x_c} \equiv \frac{\phi_{i+1,j}-\phi_{i-1,j}}{2\Delta x} \quad (7)$$

is negative, Eq. (5) is a stable operator. An implicit backward difference operator may be written for point ij as

$$-\tfrac{1}{2}\frac{(\phi_x{}^2)_{i-1/2,j}-(\phi_x{}^2)_{i-3/2,j}}{\Delta x}+\frac{(\phi_y)_{i,j+1/2}-(\phi_y)_{i,j-1/2}}{\Delta y}=0 \quad (8a)$$

or, as done previously

$$-\left(\frac{\phi_{ij}-\phi_{i-2,j}}{2\Delta x}\right)\left[\frac{\phi_{ij}-2\phi_{i-1,j}+\phi_{i-2,j}}{(\Delta x)^2}\right]+$$
$$\left[\frac{\phi_{i,j+1}-2\phi_{ij}+\phi_{i,j-1}}{(\Delta y)^2}\right]=0 \quad (8b)$$

This is a suitable first-order accurate operator for a hyperbolic equation with propagation of information in the plus x direction and can be shown to be unconditionally stable, based on a linear stability analysis, if the term in the first bracket (backward velocity formula)

$$\phi_{x_b} \equiv \frac{\phi_{ij}-\phi_{i-2,j}}{2\Delta x} \quad (9)$$

is positive.

There are two situations where a switch must be made between the elliptic and hyperbolic difference formulas. For flow accelerating through the sonic velocity, there will always be one mesh point on each j = const line for which $\phi_{x_c} > 0$ and $\phi_{x_b} < 0$ so that neither of the preceding formulas is locally stable. Thus, a parabolic point operator was introduced[4] for such sonic points by setting ϕ_x to zero to yield

$$\frac{\phi_{i,j+1}-2\phi_{ij}+\phi_{i,j-1}}{(\Delta y)^2}=0 \quad (10)$$

For flow decelerating through sonic velocity, a point on each j line will always occur for which $\phi_{x_c} < 0$ and $\phi_{x_b} > 0$ so that both formulas (5) and (8) are locally stable. In the work to date, Eq. (5) has been used at these points. In the next paragraph, a new difference formula is given for this switching situation.

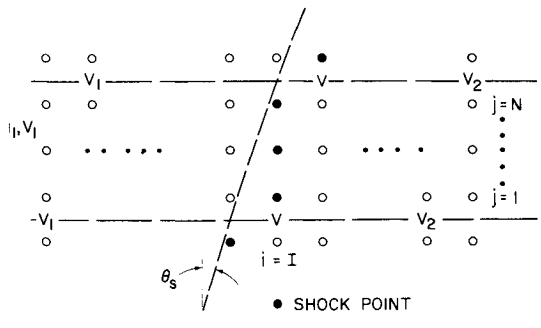

Fig. 1 Oblique shock analog for finite mesh.

Shock-Point Operator

The difference equations (5, 8, and 10) are consistent with the governing differential Eq. (1) and properly account for its changing type and local domain of dependence. Solutions of the difference equations for continuous (shock-free) flows agree with exact solutions. There is no guarantee from the analysis heretofore that the difference equations will uniquely give the correct discontinuous (weak) solution Eqs. (3) or (4). A new difference operator is now introduced that provides this guarantee.

At each mesh point where $\phi_{x_b} > 0$ and $\phi_{x_c} < 0$, the shock-point difference operator

$$-\tfrac{1}{2}\frac{(\phi_x{}^2)_{i+1/2,j}-(\phi_x{}^2)_{i-1/2,j}}{\Delta x}-\tfrac{1}{2}\frac{(\phi_x{}^2)_{i-1/2,j}-(\phi_x{}^2)_{i-3/2,j}}{\Delta x}+$$
$$\left(\frac{\phi_{y_{i,j+1/2}}-\phi_{y_{i,j-1/2}}}{\Delta y}\right)=0 \quad (11)$$

is to be used. The x differences in this operator are the sum of the x differences for the elliptic and hyperbolic operators. As noted previously, both operators are separately stable at this point, and Eq. (11) has been found to be stable by numerical tests. Equation (11) may be written in terms of ϕ by use of Eqs. (6).

The implementation of Eq. (11) is straightforward. Values for ϕ_{x_b} and ϕ_{x_c} are computed at each mesh point and, based on their values relative to zero, there are four choices for constructing the x difference operators given in Eqs. (5, 8, 10, and 11). The difference equations along an x = const line may be linearized at each iteration to form a tridiagonal diagonally dominant matrix solvable by direct elimination. Successive line relaxation is used as before with the elliptic points overrelaxed.

The terminology "shock-point operator" has been chosen since the mesh point in question will generally be near a shock. It should be noted that the use of Eq. (11) is not the same as shock fitting. No internal boundary is identified in the solution across which a discontinuous change of variables is enforced.

Normal Shock Waves

The normal shock solution $u_2 = -u_1$ is readily obtained from the difference equations by setting the y differences to zero. Equations (8, 11, and 5) then have the following possible solutions, respectively

$$\phi_{x_{i-1/2}} = \pm\phi_{x_{i-3/2}} \quad (12a)$$
$$\phi_{x_{i+1/2}} = \pm\phi_{x_{i-3/2}} \quad (12b)$$
$$\phi_{x_{i+1/2}} = \pm\phi_{x_{i-1/2}} \quad (12c)$$

Choosing the plus sign in Eqs. (12a) and (12c) and the minus sign in Eq. (12b) yields

$$u_2 = \cdots = \phi_{x_{i+3/2}} = \phi_{x_{i+1/2}}$$
$$= -\phi_{x_{i-3/2}} = -\phi_{x_{i-5/2}}$$
$$= \cdots = -u_1 \quad (13)$$

Thus the jump occurs over three mesh intervals between two uniform flows that uniquely satisfy Eq. (3).† Without the shock-point operator, the difference equations admit the correct solution[4] but also admit incorrect solutions.

Oblique Shock Waves

Consider an infinite oblique shock wave. All quantities are invariant along the direction of the shock, and the upstream and downstream states are uniform. An analog of this problem for a finite mesh is outlined in Fig. 1. The dashed line at angle θ_s represents the direction along which quantities would be invariant if the numerical solution is an accurate representation of the true solution. For reference purposes, let the location of this line be representative of the location of the true shock. From

† The correct values of ϕ_x and ϕ_y to print out are those midway between mesh points. This is inconvenient, however, since ϕ_x and ϕ_y are then not at the same point. For the results in Sec. III, the centered formulas, e.g., Eq. (7), are used. Hence, the shock jump takes four mesh points.

experience, it is known that a shock wave calculated by this method will actually be spread over several mesh points.

To illustrate the oblique-shock-wave solution, choose a mesh, as shown in Fig. 1, so that $\Delta y = \Delta x \tan\theta_s/N$ where N is an integer. By the invariance condition, values of ϕ are equal at mesh points separated by Δx in the x direction and $N\Delta y$ in the y direction. We need only consider the solution for a band of mesh points of height $N\Delta y$ such as between the two horizontal lines in Fig. 1. Along these lines, there is a periodic boundary condition

$$v_{i,j+1/2} = v_{i+1,j+N+1/2} \tag{14}$$

where v is defined by Eq. (6).

If the upstream flow is assumed to be supersonic ($\phi_{x_c} > 0$ and $\phi_{x_b} > 0$), hyperbolic difference operators would be used to march downstream from an initial data plane of uniform flow $u_1 v_1$. Eventually, some points will be reached where $\phi_{x_b} > 0$ and $\phi_{x_c} < 0$ if the downstream flow $u_2 v_2$ is assumed subsonic. These points will be called "shock points" and, for the assumed situation, they will occur in the pattern shown by the solid symbols in Fig. 1. For all mesh points downstream of the shock points, $\phi_{x_c} < 0$ and $\phi_{x_b} < 0$ and the elliptic difference operators would be used.

If the hyperbolic difference operators [Eq. (8a)] for all mesh points $i = -\infty, \ldots, I-1$ and $j = 1, \ldots, N$ are considered, they may be summed to yield

$$-\frac{1}{2}\left[\frac{1}{N}\sum_{j=1}^{N}(u^2_{I-3/2,j}) - {u_1}^2\right] + \frac{\Delta x}{N\Delta y}(v_1 - v_{I-1,1/2}) = 0 \tag{15}$$

This simple formula results because: a) all contributions between neighboring mesh points cancel since the difference equations are written in divergence form; and b) contributions from the upper and lower boundary points cancel, except at the end points, due to the periodic boundary condition, Eq. (14). Similarly, if the elliptic difference operators [Eq. (5a)] for all mesh points $i = I+1, \ldots, \infty$ and $j = 1, \ldots, N$ are considered, their sum is given by

$$-\frac{1}{2}\left[{u_2}^2 - \frac{1}{N}\sum_{j=1}^{N}(u^2_{I+1/2,j})\right] + \frac{\Delta x}{N\Delta y}(v_{I,1/2} - v_2) = 0 \tag{16}$$

The sum of the shock-point difference operators [Eq. (11)] at points $i = I$ and $j = 1, \ldots, N$ is

$$-\frac{1}{2}\left[\frac{1}{N}\sum_{j=1}^{N}(u^2_{I+1/2,j} - u^2_{I-3/2,j})\right] + \frac{\Delta x}{N\Delta y}(v_{I-1,1/2} - v_{I,1/2}) = 0 \tag{17}$$

When the difference operators for all the mesh points are summed, i.e., Eqs. (15–17) are added together, the solution is

$$\tfrac{1}{2}({u_2}^2 - {u_1}^2) + (\Delta x/N\Delta y)(v_2 - v_1) = 0 \tag{18}$$

Equation (18) is the desired result since

$$\Delta x/N\Delta y = \tan\theta_s = (dx/dy)_s \tag{19}$$

and hence the solution of the difference equation is the required shock jump, Eq. (4a). The same result is obtained when an oblique shock wave with a supersonic downstream flow is considered. In that case, all the points are hyperbolic and Eq. (15) yields Eq. (18) when $I \to \infty$. The preceding analysis, when generalized to the case of arbitrary $\Delta x, \Delta y$[6] shows that the difference equations yield the correct shock jumps as the mesh is refined.

The accuracy of the calculated jump will depend on the particular mesh spacing relative to the shock-wave angle and radius of curvature. No explicit solution analogous to Eq. (13) has been obtained for the required number of mesh points for the oblique shock jump. However, calculations presented in Sec. III show that no more than four mesh points are needed if u_2 is subsonic.

For situations where the downstream flow is supersonic, it is well known that the truncation error terms of the hyperbolic difference operator introduce numerical dissipation and dispersion that determine the shock structure. The first-order accurate operator, Eq. (8), was found[4] to be dominated by dissipation effects that smooth out shocks over 6 to 10 mesh points. However, it has excellent stability properties. Fully second-order accurate operators are dominated by dispersive effects and give poor shock structure and can lead to instabilities. Hybrid first- and second-order schemes (as introduced by Garabedian and Korn[7] and Krupp[5]) reduce the first-order truncation error and shock-wave smearing. However, it appears that the amount of dissipation required for stability and for overcoming dispersive effects will usually smear out oblique shocks with supersonic downstream states. This compromise is a weakness in the method if sharp supersonic oblique shocks are required for a particular calculation.

For previous calculations, the elliptic operator was used instead of Eq. (11). The analysis shows then that Eq. (18) is replaced by

$$-\frac{1}{2}({u_2}^2 - {u_1}^2) + \frac{\Delta x}{N\Delta y}(v_2 - v_1) = \frac{1}{2}\frac{1}{N}\sum_{j=1}^{N}(u^2_{I-1/2,j} - u^2_{I-3/2,j}) \tag{18b}$$

For certain circumstances, the right-hand side of Eq. (18b) could be zero but, in general, it will not reduce to Eq. (4a). Thus, previous methods were able to admit the correct shock jumps, but did not guarantee that such jumps would be calculated.

Consistency Condition

A basic requirement of valid finite-difference operators is that they must satisfy the consistency condition, i.e., as $\Delta x, \Delta y \to 0$, the difference equations reduce to the governing differential equations. Using a Taylor series expansion, Eqs. (5) and (8) are consistent with Eq. (1). The parabolic point operator, Eq. (10), is also consistent even though it formally reduces to $\phi_{yy} = 0$. Since the solution is continuous at the sonic line, it may be expanded as

$$\phi_x = \delta x \phi_{xx} + \tfrac{1}{2}(\delta x)^2 \phi_{xxx} + \cdots \tag{20}$$

where $\delta x \equiv x - x_{\text{sonic}}$. If Eq. (20) is multiplied by ϕ_{xx} and subtracted from $\phi_{yy} = 0$, Eq. (10) approximates Eq. (1) with truncation error $\delta x(\phi_{xx})^2$. As $\Delta x, \Delta y \to 0$, $\delta x \to 0$, and the consistency condition is achieved.

Using a Taylor series expansion, the shock-point operator, Eq. (11), equals

$$-2\phi_x \phi_{xx} + \phi_{yy} + \Delta x(\phi_x \phi_{xx})_x + \cdots = 0 \tag{21}$$

which appears to violate the consistency condition. However, this is not so. If the shock point occurs in a region of smooth recompressions, the solution is continuous and, from Eq. (20), Eq. (21) is a consistent approximation with truncation error $0(\delta x)$.

If a finite strength shock is present, the shock points coincide with the shock wave as $\Delta x, \Delta y \to 0$. Equation (1) does not hold at such a point and the usual consistency condition is not violated. Analysis of the preceding paragraphs demonstrates that at shock points the consistency condition should require that, in the limit $\Delta x, \Delta y \to 0$, the difference equations yield the correct integral properties of the governing equations. When the solution is discontinuous, this requirement is imperative.

Flux Interpretation

The finite-difference equations (5a, 8a, 10, and 11) may be interpreted as flux equations when they are multiplied by $\Delta x \Delta y$. Mesh cells can be constructed by drawing boundaries midway between mesh points. The flux equations then represent fluxes of $\phi_y \Delta x$ and $-\frac{1}{2}{\phi_x}^2 \Delta y$ across horizontal and vertical sides, respectively, of the mesh cells. [These equations can be constructed as finite-difference approximations to Eq. (2), but the interpretation is a little unclear because of the uncentered x operators.] If a group of mesh cells is considered, examination of the flux equations shows that all fluxes across internal boundaries identically cancel. Thus the total flux of ϕ_y and $-\frac{1}{2}{\phi_x}^2$ into a region of mesh cells equals the total flux out of the region in accordance with Eq. (2). Hence, the above finite-difference system may be termed fully conservative. If the shock-point operator is not included, some fluxes across internal boundaries do not identically cancel when the difference

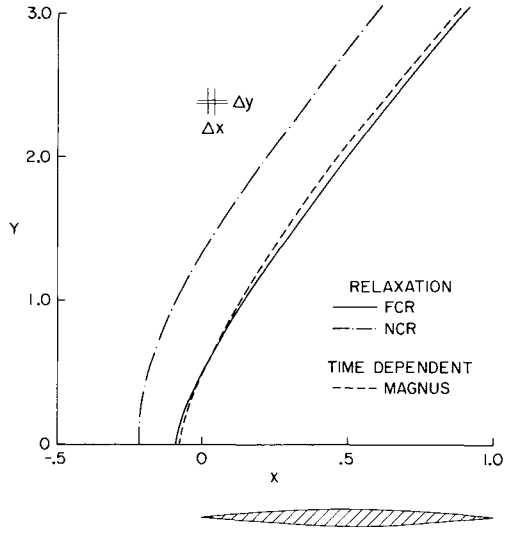

Fig. 2 Comparison of computational methods for 6% parabolic arc with detached bow wave; $M_\infty = 1.15$.

operators are switched. This gives rise to some spurious sink-like terms represented by the right-hand side terms of Eq. (18b). Thus the system of difference equations without the shock-point operator is not fully conservative for a finite mesh. For an infinitesimal mesh ($\Delta x, \Delta y \to 0$), the sink terms may have a finite strength if a shock is present.

III. Computed Examples

The first example discussed here was computed using the Guderly form of the transonic small-disturbance equation

$$-(\gamma+1)(\phi_x+u_\infty)\phi_{xx}+\phi_{yy}=0 \tag{22}$$

with $C_p = -2\phi_x$. In the remaining examples, the governing equation was solved in the similarity form

$$(K-(\gamma+1)\phi_x)\phi_{xx}+\phi_{\tilde{y}\tilde{y}}=0 \tag{23}$$

where

$$K=(1-M_\infty{}^2)/(M_\infty\delta^{2/3}), \quad \tilde{y}=\delta^{1/3}M_\infty{}^{1/2}y$$
$$\bar{C}_p=(\delta^{2/3}/M_\infty{}^{3/4})^{-1}C_p=-2\phi_x$$

and δ is the body thickness ratio.

The accuracy of the shock jumps can best be assessed by comparison with the shock polar equation in the hodograph plane. For shocks in nonuniform flowfields, the comparisons are facilitated by reducing Eq. (3) to the normalized form

$$27(2+\bar{u}_2)\bar{u}_2{}^2-32\bar{v}_2{}^2=0$$

In these variables, all shocks have the upstream state $\bar{u}_1=\bar{v}_1=0$. Sonic velocity corresponds to $\bar{u}=-1$, and the normal shock is given by $\bar{u}_2=-2$, $\bar{v}_2=0$. The maximum turning angle for all shocks is $\bar{v}_2=1$ and occurs with $\bar{u}_2=-\frac{4}{3}$. For the above similarity form of the equation

$$\bar{u}\equiv\frac{\gamma+1}{-K_1}(\phi_x-\phi_{x_1})$$
$$\bar{v}\equiv\left(\frac{3}{-K_1}\right)^{3/2}\frac{\gamma+1}{4}|\phi_y-\phi_{y_1}|$$
$$K_1\equiv K-(\gamma+1)\phi_{x_1}$$

An exact solution along a physical (xy) streamline crossing a shock would appear in the hodograph plot as a discontinuous jump form $\bar{u}_1=\bar{v}_1=0$ to $\bar{u}_2\bar{v}_2$ satisfying the above, followed by a continuous varition of $\bar{u},\bar{v}$ downstream of the shock.

For the numerical solutions, upstream conditions ϕ_{x_1}, ϕ_{x_2} are defined and values of $\bar{u}$, $\bar{v}$ are plotted along the $y=$ const line (streamline) downstream of this point. Several mesh points are required to make the shock jump. The downstream state is identified by a change in direction of the $\bar{u},\bar{v}$ trajectory and, for a good solution, should lie near the polar.

Results calculated by the method outlined in Sec. II *with* the shock-point operator are termed "fully conservative relaxation" (FCR) solutions. Results calculated *without* the shock-point operator are termed "not fully conservative relaxation" (NCR) solutions. Unless otherwise noted, results presented below are calculated with the FCR method.

Detached Bow Shock

A detached bow-wave calculation is well suited for examining the shock jumps since the upstream flow is uniform and all possible shocks from normal to weak oblique are present. The flow past a 6% parabolic arc with $M_\infty = 1.15$ ($u_\infty = 0.12029$) was calculated by the two relaxation methods and one time-dependent (TD) method. The same governing equation [Eq. (22)]

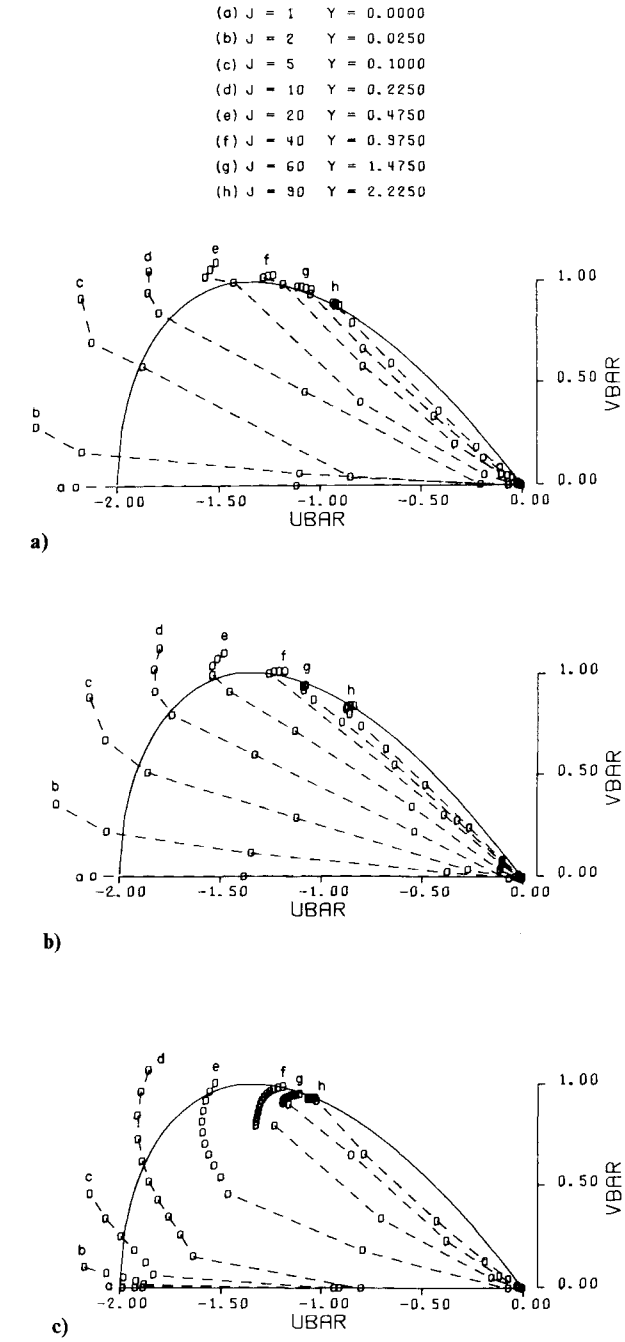

Fig. 3 Hodograph plots for detached bow wave: a) fully conservative relaxation; b) time-dependent (Magnus); and c) not fully conservative relaxation.

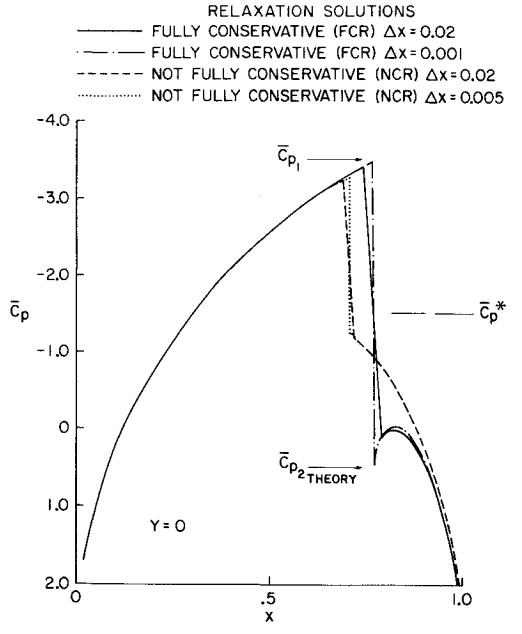

Fig. 4 Pressure distribution for parabolic arc airfoil, $K = 1.8$.

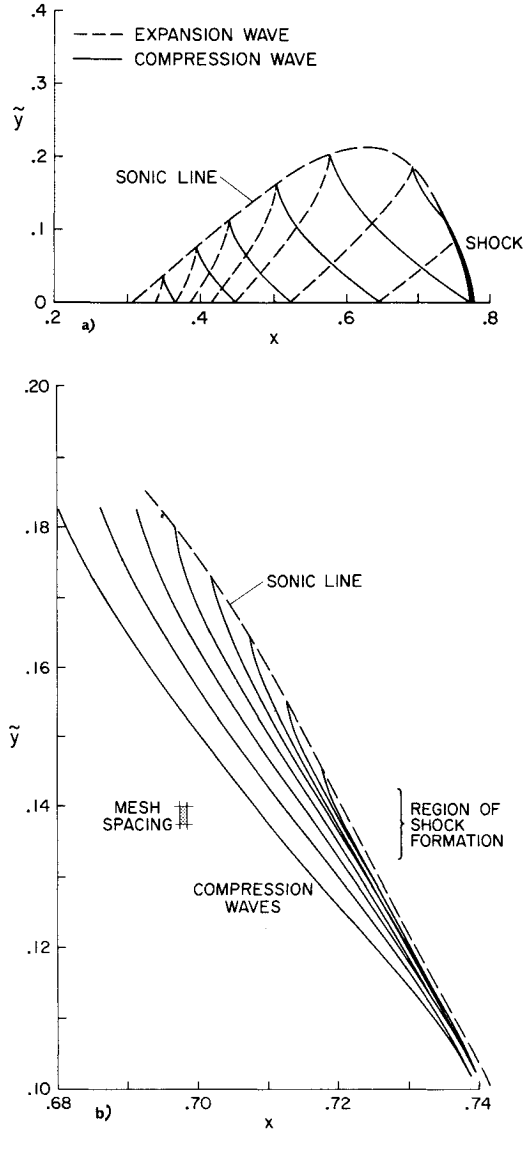

Fig. 5 Structure of embedded supersonic region. Parabolic arc airfoil, $K = 1.8$: a) over-all; and b) detail near shock tip.

and the same boundary conditions were used for all three calculations which, in addition, were done on the same mesh ($\Delta x = \Delta y = 0.025$, $-0.2875 \leqq x \leqq 1.1125$, $0 \leqq y \leqq 3.0$). For the relaxation calculations, the ϕ equation was used and the problem formulation follows that of Ref. 8. The TD calculations were performed by R. Magnus[9] using a diffusive two-step, Lax-Wendroff method for the u, v equations.

The positions of the detached bow waves are shown in Fig. 2. Essentially the same result is obtained by the TD and FCR methods while the NCR method calculates a bow shock with too great a detachment distance. (The bow-shock position is defined by the point of maximum $\Delta C_p/\Delta x$). Shock jump for the three calculations are shown in the hodograph plots of Figs. 3a–c. Solutions for the TD and FCR methods compare reasonably well with the exact solution and with each other. The main discrepancies are near the $y = 0$ axis where the downstream side of the shock is immersed in the stagnation-point flowfield. Accuracy in this region can be improved by mesh refinement (one case was computed with the FCR method for $\Delta x = 0.0125$).‡ In Fig. 3c shock jumps for the NCR method are considerably in error for the strong oblique shocks, but are reasonably good for the normal and weak oblique shocks. The principal difference between the time-dependent and fully conservative relaxation methods is the required computing time, the latter being an order of magnitude faster on the same machine.[1] Including the shock-point operator greatly improved the convergence properties of the relaxation calculation and eliminated the slow convergence noted in Ref. 8.

Embedded Shock Over Airfoil

An example of a subsonic flow with an embedded supersonic region and shock wave is displayed in Figs. 4–6 for a parabolic arc at zero incidence. The NCR solution (Fig. 4) was originally presented in Ref. 2 wherein it was noted that the shock pressure rise was less than the theoretical value. The discrepancy was attributed to a smearing out of the re-expansion singularity. Solutions with the FCR method show that, with a fine mesh near the shock, the theoretical normal shock pressure rise is

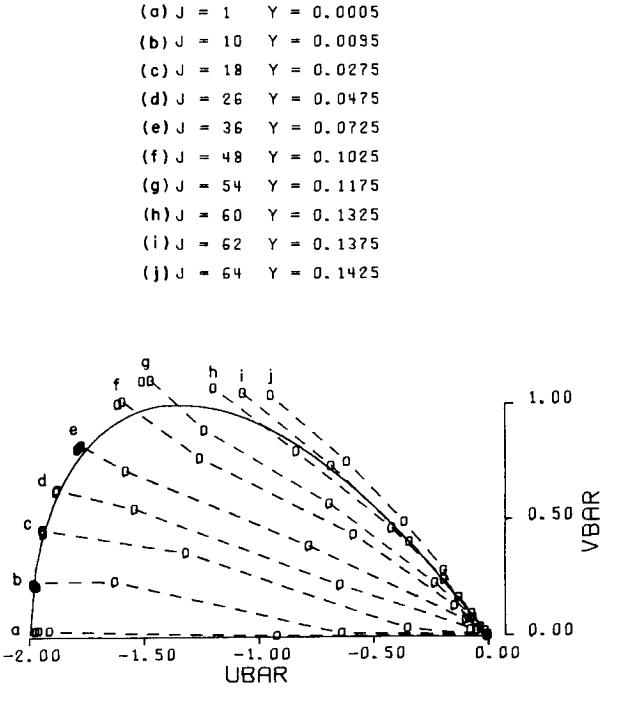

Fig. 6 Hodograph plot for embedded shock. Parabolic arc airfoil, $K = 1.8$.

‡ The normal shock jump for the relaxation methods is considerably better if ϕx midway between mesh points is used (see previous footnote).

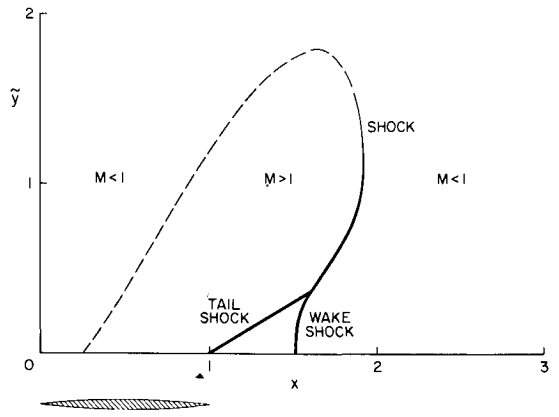

Fig. 7 Flowfield features—parabolic arc airfoil, $K = 0.81$.

attained and the singularity is well defined. The NCR solution, computed on the same coarse mesh as the FCR solution and also on a fine mesh, does not produce the normal shock jump. The shock wave computed by the FCR method is stronger than, and aft of, the one using the earlier NCR method. This trend has generally been observed in the calculations to date.

Flowfield features of the embedded supersonic zone are shown in Fig. 5. The shock is formed by compression waves reflected from the sonic line. Details of this process near the shock tip are illustrated in Fig. 5b. Above about $\tilde{y} = 0.14$, the reflected compression waves do not coalesce and the recompression to subsonic flow is continuous. Below this point, the waves coalesce to form a shock wave that is continuously strengthened until it reaches the surface (shown schematically by the thickening shock in Fig. 5a). This description corresponds to the deductions from hodograph theory.[10] The exact structure at the tip of the shock wave cannot be resolved with the present mesh.

Figure 6 shows a series of representative hodograph streamlines through the shock. The normalized turning angle $\bar{v}$, which is zero at $\tilde{y} = 0$, varies continuously along the shock length so that an entire family of oblique shocks is traced out. In the lower portion of the shock, the solution jumps in four mesh points to close to the theoretical value. As the shock tip is approached, however, the solution deviates from the polar for the reasons noted above.

Lambda Type Shock

If K is reduced sufficiently (M_∞ increased) from the preceding value, the embedded shock wave moves aft of the body and an additional "tail" is formed by the trailing-edge turning angle (Figs. 7–9). The tail shock has supersonic downstream flow (Figs. 8 and 9a) and is weakened along its length by expansion waves from the body surface. The "wake" shock is normal at $\tilde{y} = 0$ but becomes quite oblique (Fig. 9b) before it intersects the tail shock. The "combined" shock is initially oblique, then it becomes approximately normal and then oblique again before the tip is reached (Fig. 9c). The latter two shocks are formed by compression waves reflected from the sonic line. Reflected compression waves also reach the $y = 0$ axis aft of the body, causing mild recompression ahead of the wake shock (Fig. 8). They are reflected from the axis as compression waves and will coalesce with the tail shock if distances are large enough. The structure of the flowfield generally follows that suggested by Barish and Guderly.[10]

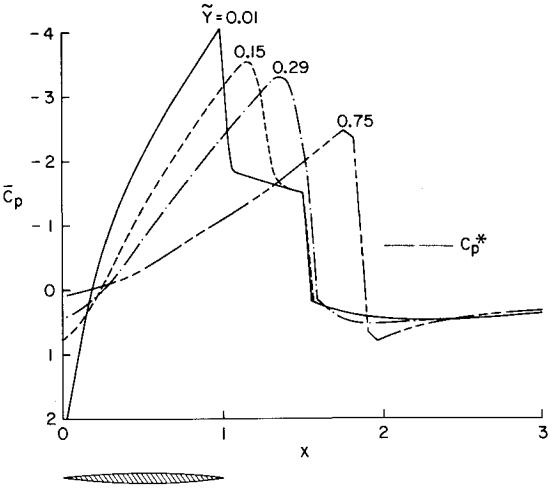

Fig. 8 Pressure distributions. Parabolic arc airfoil, $K = 0.81$.

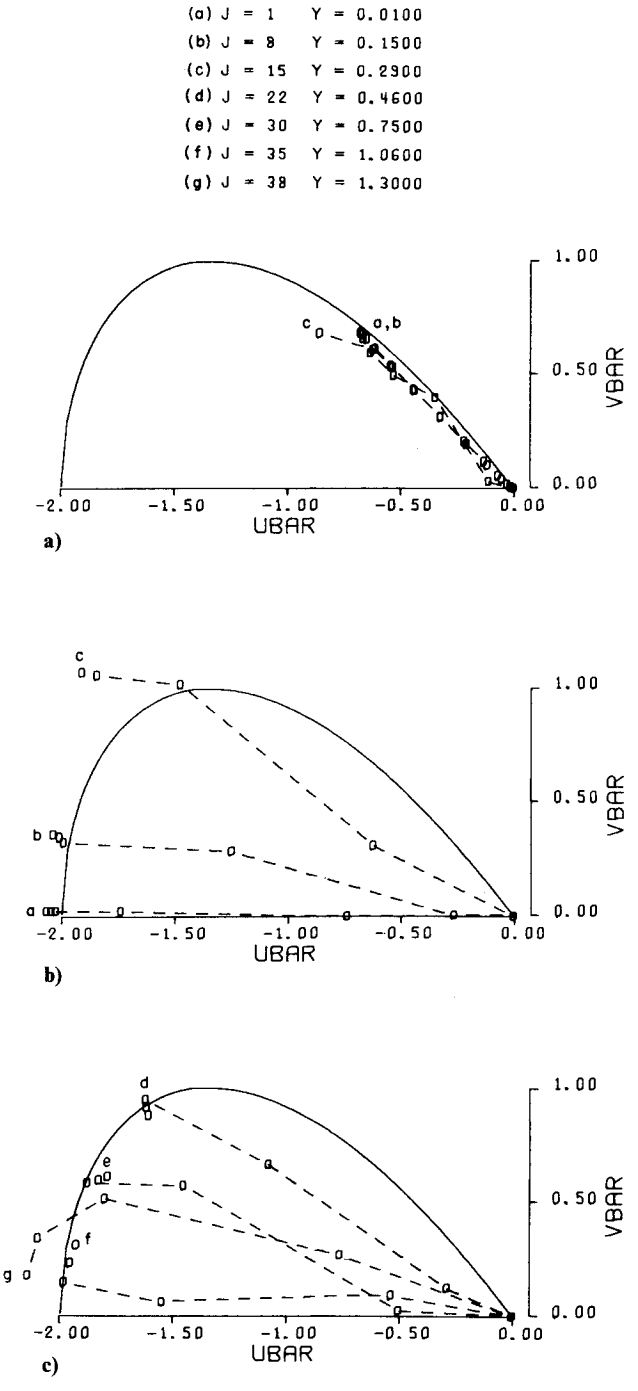

Fig. 9 Hodograph plots for embedded shocks. Parabolic arc airfoil, $K = 0.81$: a) tail shock; b) wake shock; and c) combined shock.

The tail shock is smeared out (Figs. 8 and 9a) by the numerical viscosity of the hyperbolic difference operator. Consequently, the region of shock intersection is too diffuse to analyze in detail. An analysis of a similar intersection for uniform upstream flow is given by Guderly.[10]

Shock-Free Recompression

Examples of continuous supersonic recompression are contained in the previous two examples. The calculation for a Korn shock-free airfoil reported in Ref. 4 was repeated using the FCR method. The FCR solution agreed essentially with the earlier NCR solution.

Comparison with Experimental Data

Figure 10 compares solutions using the two relaxation methods and the data of Knechtel.[11] The solution using the FCR method has a stronger shock that is considerably farther aft than the one computed by the NCR method.[2] In light of the present findings, the forward location of the shock wave for the NCR solution cannot be attributed to the re-expansion singularity. There are several possible reasons why the FCR solution gives a shock well aft of the measured location. The test Reynolds number is low and the pressure distribution indicates a laminar or transitional boundary-layer shock-wave interaction. The computed shock Mach number of 1.29 is large enough that the small-disturbance shock jump is 15% greater than the Rankine-Hugoniot jump. Comparison with the calculation of Grossman and Moretti[12] indicates that this would move the shock wave upstream. Finally, the wind-tunnel-wall interference in the experiments is of the open-jet type.[11]

In Fig. 11, solutions using the two relaxation methods are compared with the data of McDevitt and Taylor for flow past an axisymmetric body with a maximum thickness at $x = 0.3$. The formulation of this problem and results for the NCR method are reported in Ref. 13. The NCR and FCR methods give essentially the same results for this case when the same mesh is used. However, when the mesh is refined, the re-expansion singularity is clearly resolved with the FCR solution. All three calculations agree well with the data, both on and off the body. The shock wave is considerably weaker and farther forward, and the test Reynolds number is an order of magnitude larger in this example compared to the Knechtel data.

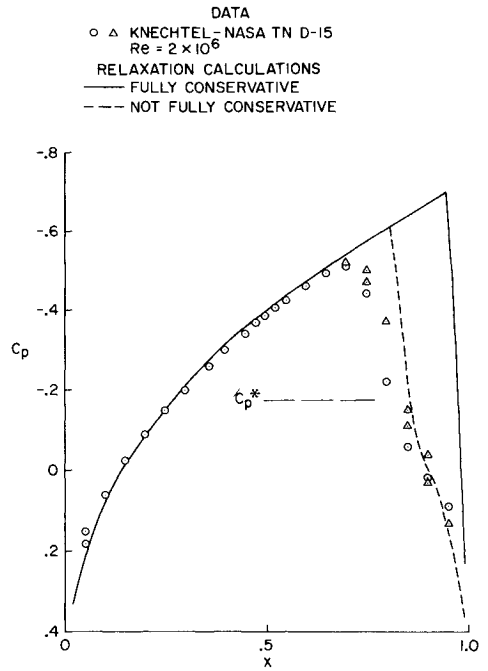

Fig. 10 Comparison of theory with data. 6% parabolic arc airfoil, $M_\infty = 0.909$.

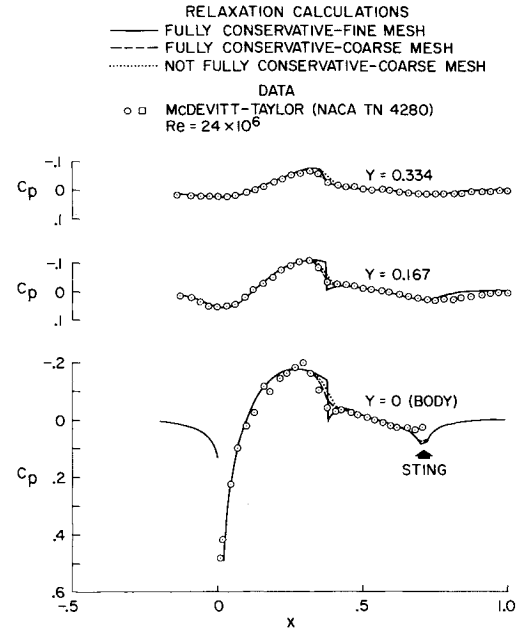

Fig. 11 Comparison of theory with data. 8.3% thick body of revolution, $M_\infty = 0.975$.

IV. Conclusions

A sufficiency condition has been derived for calculating the correct shock jumps by type dependent, finite-difference methods, i.e., a) the difference equations are written for the divergence form of the governing differential equations and are consistent with them for continuous solutions; b) the integral properties of the governing equations are preserved when switching difference operators; and c) the difference equations must be stable. Condition (b) leads to a shock-point difference operator that imposes a consistency condition for the integral equation, but not the differential, at the shock points. There may be other ways of guaranteeing the correct shock jumps (aside from shock fitting), but the author has not realized any to date. The simple solution for the normal shock jump, Eq. (13), does not result for difference equations in nondivergence form.

The particular form of the shock-point difference operator, in general, will depend on the forms of the elliptic and hyperbolic difference operators and governing equations used. The extension of the above to variable mesh is given in Ref. 6. Shock-point operators for other forms of the transonic equation are directly obtainable from Eq. (11). Other governing equations would have to be analyzed separately, however.

Examination of the calculated jump conditions confirms the analysis for a variety of shocks from normal to weak oblique. A calculation using the present relaxation techniques and a two-step, Lax-Wendroff method for a detached bow wave is shown to be in essential agreement. With adequate mesh refinement, the re-expansion singularity is well defined aft of a normal shock on a curved surface. Comparisons with earlier calculations with embedded shocks show that present solutions give stronger shocks that are farther aft on the airfoil.

References

[1] Yoshihara, Y., "A Survey of Computational Methods for 2D and 3D Transonic Flows with Shocks," GDCA-ERR-1726, Dec. 1, 1972, Convair Aerospace Division, General Dynamics, San Diego, Calif.

[2] Murman, E. M. and Cole, J. D., "Calculation of Plane Steady Transonic Flows," *AIAA Journal*, Vol. 9, No. 1, Jan. 1971, pp. 114–121.

[3] Oswatitsch, K. and Zierep, J., "Das Problem des Senkrechten Stosses an Einer Gekrümmten Wand," *Zamm*, Vol. 40, Suppl.. 1960, pp. T143–144.

[4] Murman, E. M. and Krupp, J. A., "Solution of the Transonic Potential Equation Using a Mixed Finite Difference System," *Lecture Notes in Physics*, Vol. 8, Springer-Verlag, Berlin, 1971, pp. 199–206.

[5] Krupp, J. A., "The Numerical Calculation of Plane Steady Transonic Flow Past Thin Lifting Airfoils," Ph.D. thesis, June 1971, Univ. of Washington, Seattle, Wash.

[6] Murman, E. M. "Analysis of Embedded Shock Waves Calculated by Relaxation Methods." *Proceedings of the AIAA Computational Fluid Dynamics Conference*, Palm Springs, Calif., July 1973, pp. 27–40.

[7] Garabedian, P. G. and Korn, D. G., "Analysis of Transonic Airfoils," *Communications of Pure and Applied Mathematics*, Vol. XXIV, 1971, pp. 841–851.

[8] Murman, E. M., "A Relaxation Method for Calculating Transonic Flows with Detached Bow Shocks," *Lecture Notes in Physics*, Vol. 19, Springer-Verlag, Berlin, 1973, pp. 201–205.

[9] Magnus, R. M., "The Direct Comparison of the Relaxation Method and the Pseudo-Unsteady Finite Difference Method for Calculating Steady Planar Transonic Flow," TN-73-SP03, 1973, General Dynamics, Convair Aerospace Division, San Diego, Calif.

[10] Guderly, K. G., *The Theory of Transonic Flow*, Pergamon Press, New York, 1962.

[11] Knechtel, E. D., "Experimental Investigation at Transonic Speeds of Pressure Distributions Over Wedge and Circular-Arc Airfoil Sections and Evaluations of Perforated-Wall Interference," TN D-15, 1959, NASA.

[12] Grossman, R. and Moretti, G., "Time Dependent Computation of Transonic Flows," AIAA Paper 70-1322, Houston, Texas, 1970.

[13] Krupp, J. A. and Murman, E. M., "Computation of Transonic Flows Past Lifting Airfoils and Slender Bodies," *AIAA Journal*, Vol. 10, No. 7, July 1972, pp. 880–886.

MAY 1974 AIAA JOURNAL VOL. 12, NO. 5

Approximate Method for Estimating Wake Vortex Strength

JOHN E. FIDLER*
Martin Marietta Aerospace, Orlando, Fla.

An approximate method is presented for estimating the strength of slender-body wake vortices. The method is shown to yield good accuracy for the case of asymmetric vortices in the wake of a body at high angle of attack.

Nomenclature

A = area of wake vortex cross section
C_p = pressure coefficient
d = body diameter
F = vorticity flux
g = body length from which boundary-layer fluid is shed to form single vortex
k = dimensionless velocity parameter
M = Mach number
dl = elementary length vector in plane of A
$\bar{q}$ = general velocity vector
Re = Reynolds number
U = circumferential component of velocity at boundary-layer edge
u = circumferential component of velocity in boundary layer
V = freestream velocity
$\bar{w}$ = general vorticity vector
x = distance parallel to body axis
y = distance normal to surface
α = angle of attack
δ = boundary-layer thickness
θ = angle around circumference, measured from windward side meridian
ξ = angle between vortex cores and body axis
Γ = vortex strength
Γ_P = vortex strength parameter
χ = quantity associated with vortex core angle, $= \tan\xi/\tan\alpha$

Subscripts
B = from body
a = along vortex core
c = crossflow
s = separation
V = in vortex

Superscript
* = critical value

Received October 9, 1973; revision received December 18, 1973.
Index categories: Jets, Wakes, and Viscid-Inviscid Flow Interactions; Viscous Nonboundary-Layer Flows; LV/M Aerodynamics.

* Staff Engineer.

Introduction

A MAJOR problem in missile aerodynamics is posed by the separation and subsequent behavior of the boundary layers on various missile components. This is particularly so when the separated flow forms large, powerful wake vortices whose effect on downstream components can be severe. A well-known example is furnished by the vortices in the wake of a slender axisymmetric body at incidence. These vortices first appear, at

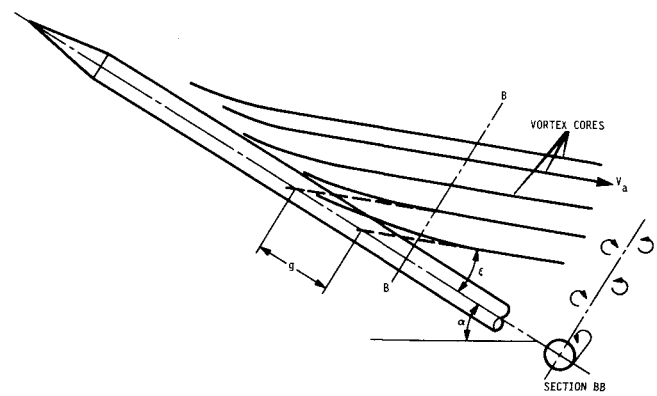

Fig. 1 Schematic of lee side vortex pattern.